Characterization of (La,Sr)(Ti,Co)O3 Oxides for Symmetrical Solid Oxide Fuel Cell Electrodes

F. Napolitano[a], A. Soldati [a], J. Geck[b], L. Suescun[c], L. Acuña[d], A. Fernandez Zuvich[a], D.G. Lamas[e], A. Serquis[a]

[a] CONICET – Centro Atómico Bariloche, S. C. de Bariloche (R8402AGP), Argentina
[b] Leibniz Institute for Solid State and Materials Research IFW Dresden, Dresden, Germany
[c] Cryssmat-Lab, Facultad de Química, Universidad de la República, Montevideo, Uruguay
[d] CINSO – Centro de Investigaciones en Sólidos, CITEDEF-CONICET, Villa Martelli, Argentina
[e] Laboratorio de Caracterización de Materiales, Facultad de Ingeniería, Universidad Nacional del Comahue, Neuquén, Argentina

In this work, a combined synchrotron X-ray diffraction (XPD), X-ray absorption near edge spectroscopy (XANES) and Extended X-ray Absorption Fine Structure (EXAFS) study of LSTC ($0 \leq y \leq 0.5$), intended as symmetric solid oxide fuel cells electrode, is presented. Charge compensation mechanisms were characterized by room temperature measurements; LSTC has a perovskite pseudocubic structure with an A-site vacancy concentration related with Co doping level. This result seems to be triggered by the fact that Ti remains in a higher formal valence (around 4+) independent of the Co concentrations. On the contrary, Co K-edge XANES spectra shows a dependency with the doping level but this seems to be related to structural changes. In-situ measurements simulating SSOFC working environment show that LSTC undergoes a rhombohedric to cubic perovskite phase transition with critical temperature being dependent of the structural distortion level.

Introduction

The Symmetrical Solid Oxide Fuel Cells (SSOFCs) is a subtype of SOFC where the same material is used as anode and cathode simultaneously (1, 2). This new approach could solve two of the main Fuel Cells problems, sulfur poisoning and carbon deposits when the cell is using hydrocarbon as fuel, by simply inverting the gas flux. Besides, this design should be less complicated than the conventional fuel cells due to the smaller number of components.

(La,Sr)TiO_3 (LST) has been widely reported as a possible SOFC anode material (3) and oxides based on this compound are also between the few reported as possible electrode materials for SSOFCs (4). Meanwhile, at SOFC cathode side, (La,Sr)CoO_3 (LSC) is a well-studied perovskite with excellent electrochemical properties (5) making the solid solution LST-LSC a good candidate for SSOFC electrode. The lack of a good

structural characterization on this solid solution is being solved in several steps beginning with the characterization at room temperature (6, 7). In this work we used synchrotron based techniques to characterize the crystal and electronic structure in Co doped LST (LSTC). This knowledge is fundamental in the design and optimization of the material´s electrochemical behaviour for SSOFC applications.

Experimental

We investigated the perovskite family $La_{0.4}Sr_{0.6}Ti_{1-y}Co_yO_{3\pm\delta}$ with $0.0 \leq y \leq 0.5$ (LSTC) prepared by a chemical route of citrates and sintered at 750 and 1100 °C (grain size about 40 and 500 nm, respectively).

Powder X-ray diffraction measurements were performed at the D10B-XPD beamline of the LNLS with 10 keV energy (λ = 1.240232 Å) between 15 and 85 degree in 2θ range using a Mythen 1K detector, at 25, 200, 400 and 750 °C under both synthetic air and 5%H2/95%N2 atmospheres (100 ml/min). Meanwhile, in-situ experiments were carried out during the heating and cooling ramps (10 °C/min) leaving the detector centered at 2θ = 31.8° and continuously collecting scans (20 seconds each) in order to follow a rhombohedric to cubic phase transition. Furnace calibration was carried out through temperature dependent XPD measurements of an MgO standard. Space group determination and Rietveld refinements were performed combining Fullprof Suite and Bilbao Crystallographic Server tools.

X-ray absorption measurements were performed at the D04B-XAFS1beamline of the LNLS. The powder samples were diluted with BN in ratio 1:5 (to get an absorption integral of 1 in the Co and Ti K-edges) and then pressed as pellets. XANES spectra were taken from 200 eV below to 800 eV above each K absorption edge using a Si(111) monochromator crystal (Co K-edge: 7709 eV, Ti K-edge: 4966 eV). The measurements were carried out in transmission mode at room temperature. Energy steps between 0.1 and 1 eV were used for the XANES and EXAFS regions, respectively. At least three scans were measured for each sample in order to optimize signal-to-noise ratio. A Metallic (Ti or Co) foil was used in each case as a reference for energy shift calibration. Co and Ti references materials with different oxidation states were prepared and measured with the same procedure.

Results and Discussions

Structural Characterization

Diffractograms acquired over samples synthesized at 1100 °C show all reflections belonging to the cubic and rhombohedral perovskite phases (see Figure 1 in reference (6)).

Structural parameters were obtained from Rietveld refinements of room temperature measurements. The passage from the cubic (Pm-3m, y = 0.0 sample) to the rhombohedric structure (R-3c, $0.0 < y \leq 0.5$) is due to the freezing of the $R5^-$ symmetry mode, related to

the oxygen octahedra rigid rotation. The best refinement indicated an A-site deficient perovskite structure for low Co content samples ($y \leq 0.3$) due to segregation of Sr from the inner structure. This result is in agreement with previously reported results for a low temperature synthesized undoped titanate (8, 9). The LSTC A-site vacancies and the cobalt concentration are inversely correlated (Figure 1); a remarkable Sr increment is observed at $0.0 \leq y \leq 0.3$ range, tending to the stoichiometric theoretical value of 0.6 and, in the case of $y = 0.0$ sample, Sr content is consistent with $La_xSr_{1-3/2x}TiO_3$ compounds (reported for low temperature synthesis).

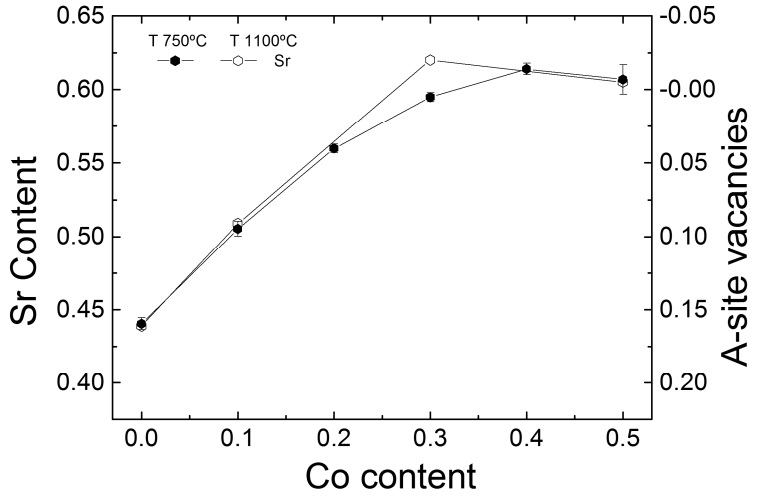

Figure 1. Sr content and number of A-site vacancies calculated from Rietveld refinements in two LSTC series (synthetized at 750 and 1100ºC respectively).

The LSTC lattice parameter evolution with Co doping level (shown in reference (6)) has a relatively stable value for the low Co content range ($0.0 \leq y \leq 0.3$). This range coincides with the compositions for which A-site vacancies creation is the active charge compensation mechanism in this system. Sample grain size (indirectly evaluated by the synthesis temperature) showed no influence over structural parameters at room temperature.

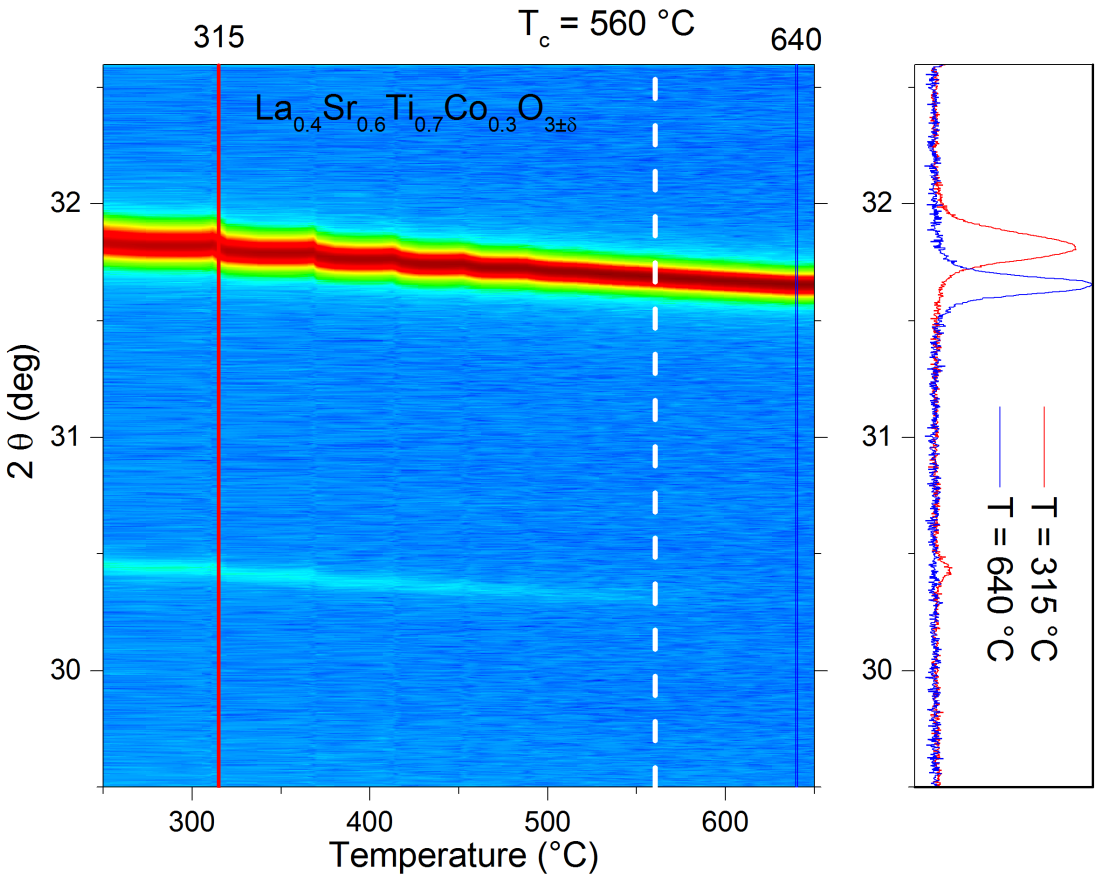

Figure 2. Short diffraction patterns corresponding to $La_{0.4}Sr_{0.6}Ti_{0.7}Co_{0.3}O_{3\pm\delta}$ sample synthesized at 1100 °C, measured as temperature was increased from 25 up to 790 ºC at 10 ºC/min in synthetic air (only the interesting range of temperature is displayed). Profiles at 315 and 640 ºC are detailed at the right, showing the rhombohedric and the cubic phase, respectively.

High temperature X-ray diffraction experiments were performed on LSTC samples with y = 0.1, 0.3 and 0.5 from room temperature up to 750 °C. On all samples a reversible rhombohedric to cubic phase transition was observed under both oxidizing and reducing atmospheres, again related to the $R5^-$ symmetry mode. In-situ measurements were carried out looking at 29.40° - 33.0° 2θ range in order to follow the evolution of two peaks: the first one, at 30.6°, associated to the (113) reflection of the rhombohedral phase (forbidden in the cubic symmetry) and the second one at 32.0° that is due to an overlapping between (202) and (006) reflections, both merging into the (111) reflection of the cubic phase. Results from the LSTC with y = 0.5 sample in synthetic air is displayed in Figure 2 where the sample symmetry is gradually increased with the temperature, observed as a decreasing intensity in the (113) reflection and the increasing overlapping between the (202) and (006) reflections. Both observations could be taken as a flag of the rhombohedric to cubic phase transition. These results are representative for all LSTC samples measured in synthetic air.

Transition temperature was found to be dependent of the rhombohedric distortion level at room temperature (e.g. y = 0.3 sample shows the higher distortion level and the higher transition temperature) measured by the amplitude of the $R5^-$ symmetry mode (see Table 1).

TABLE 1. Relationship between strcutrual distortion (at room temperature) and phase transition temperature in $La_{0.4}Sr_{0.6}Ti_{1-y}Co_yO_{3\pm\delta}$.

Sample	y	|R5⁻|	T_c (ºC)
LSTC01-1-1100	0.1	0.38(2)	370
LSTC03-1-1100	0.3	0.407(8)	560
LSTC05-1-1100	0.3	0.25(3)	310

Same results were obtained from low temperature synthesized LSTC samples, although the phase transition was more difficult to follow due the broadening and the low intensity of the (113) reflection. The transition temperature observed in these samples were considerably lower (220, 270 and 225 °C for y = 0.1, 0.3 and 0.5 samples, respectively).

Transition Metal Local Environment

Local environments around Ti and Co were studied by EXAFS data refinements, analyzing in particular their first coordination spheres. All the LSTC samples showed the same characteristic Fourier transform around the first coordination sphere (Ti and Co measurements), where no distortion of the oxygen octahedral is noticeable. This result is in concordance with the long range crystallographic model found by X-ray diffraction. The EXAFS signal Fourier transform of the LSTC sample with y = 0.3 along with its corresponding first sphere refinement is presented in Figure 3, as an example.

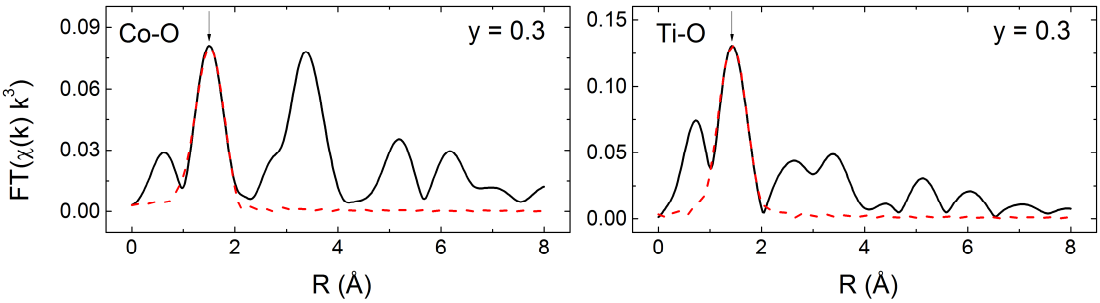

Figure 3. Fourier transform and first coordination sphere fit of LSTC sample with y=0.3 for Cobalt and Titanium K-edge absorption. The arrows point to the first coordination shells.

A remarkable difference was found between Ti-O and Co-O distances results. The Co-O distance decreases as Co content in the sample is increased but the Ti-O remains invariant along the whole LSTC compositional series (Table 2).

TABLE 2. Metal-oxygen distances at the first coordination shell, measured by EXAFS in three LSTC samples.

Distance	y = 0.1	y = 0.3	y = 0.5
Ti-O	1.91 (1)	1.91 (1)	1.91 (1)
Co-O	2.04 (1)	1.95 (1)	1.92 (1)

Electronic Configuration

The cobalt absorption coefficient in the LSTC samples and two reference materials ($LaCoO_3$ and $La_{0.5}Sr_{0.5}CoO_3$) presents a main absorption jump between 7705 and 7725 eV. The white line (WL) appears due to 1s-4p electrical dipole transitions. The edge energy is defined as the position of the first maximum of the absorption spectra first derivative.

In the LSTC series, two main changes in the Co K-edges XANES spectra can be observed as Co content is increased: the edge position moves to higher energy and the WL decreases (Figure 4, top). On the contrary, the Ti XANES K-edge spectra do not show any appreciable changes as a function of the doping level (Figure 4, bottom) staying close to the $SrTiO_3$ edge energy (Ti^{4+} reference).

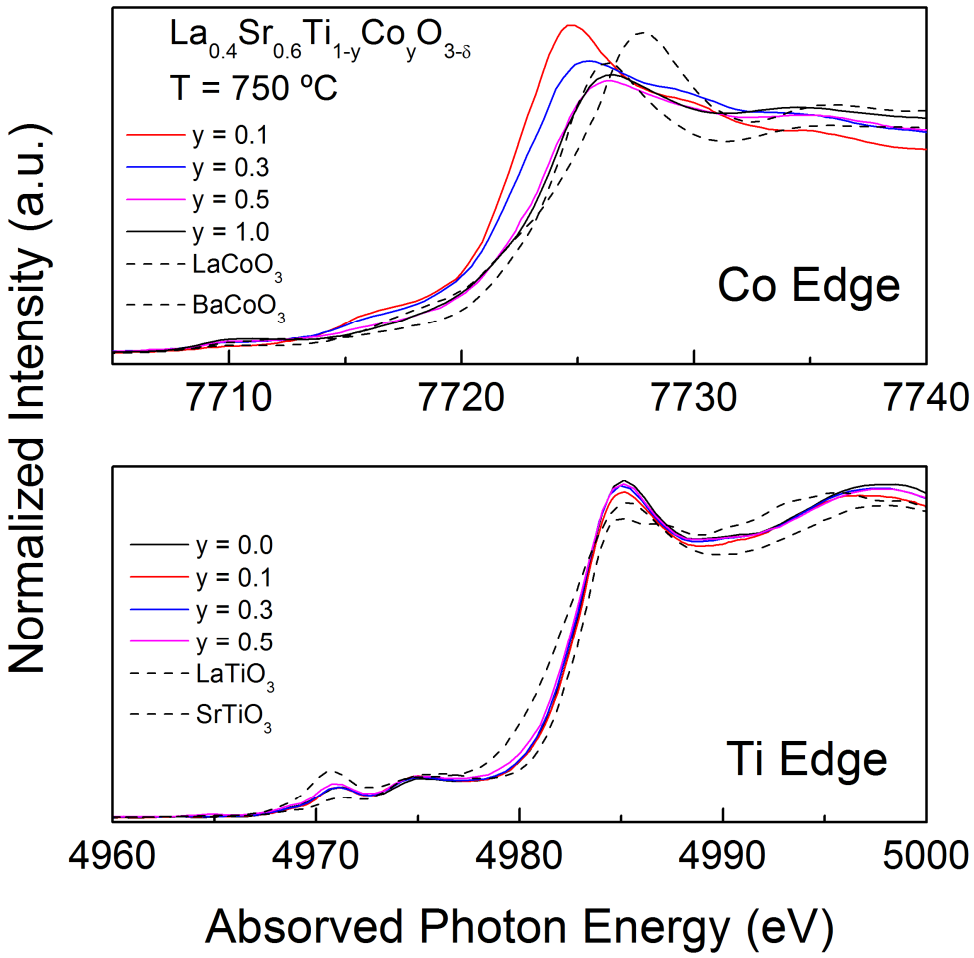

Figure 4. $La_{0.4}Sr_{0.6}Ti_{1-y}Co_yO_{3\pm\delta}$ ($0.0 \leq y \leq 0.5$) normalized X-ray absorption spectra around Co (top) and Ti (bottom) K-edge absorption edge for samples synthesized at 750 °C. Standard samples with a well-known transition metal oxidation state are also drawn (dashed lines) for comparison purpose.

It is commonly accepted that the position of the transition metals (TM) K-edges is, among other factors, related to its average valence. This fact motivates the attempt to determine the oxidation state of Co as a function of its concentration in LSTC samples. However, it is also well known that the absorber local environment is affected by the crystal field, and in this way the TM K-edge position may vary from the expected values

for a given oxidation state. That means that any effect of structural modification along the compositional LSTC series on the electronic structure has to be discarded before the K-edge energy position and absorber valence state calibration could be carried out .

Theoretical DFT calculations using the results from EXAFS local structure as input indicate that the Co-O distance variation along the LSTC series has a strong influence over crystal field, therefore affecting directly the Co K-edge energy position. Indeed, a shift of 1.6 eV is observed in the calculated Co K-edge XANES spectra between two samples (Figure 5). It is worth to note that also the decreasing intensity in the WL is well reproduced in this model.

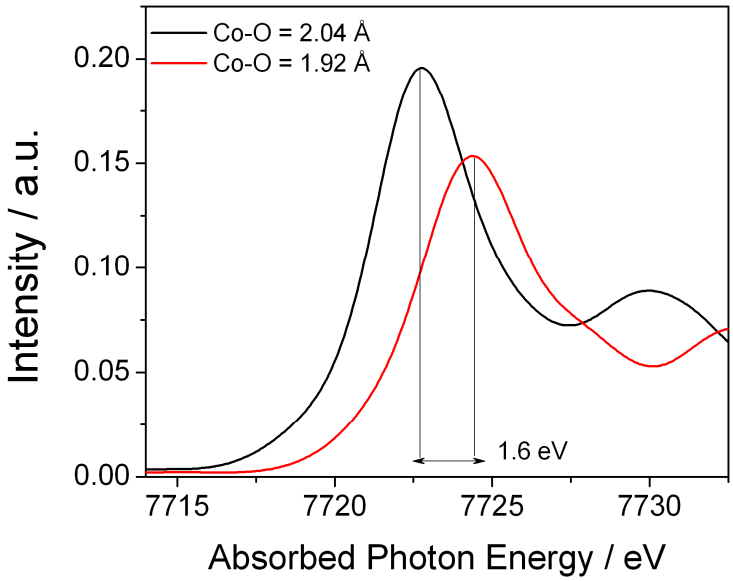

Figure 5.The p-projected Co-DOS as determined by DFT- The DOS is up-shifted by 7.709 keV and broadened by 1 eV, in order to facilitate comparison to the experimental data.

This result indicates that the calibration of Co K-edge energy position with the Co valence state is not straightforward. Taking into account the position of the XANES first derivative from LSTC and standard samples we identify Co being near 3+ valence state. However, due to the reasons mentioned before, no fine calibration can be done inside the sample's series. In contrast, as Ti-O distance maintains a stable value along the compositional range, the structural effect in the Ti K-edge position can be neglected and thus, the calibration should be valid for the whole set of samples. The Ti K-edge analyses yield that Ti remains in a high valence state (Ti^{4+}), independently of the Co doping level.

Conclusions

Perovskite-type $La_{0.4}Sr_{0.6}Ti_{1-y}Co_yO_{3\pm\delta}$ (LSTC) oxides, candidates for symmetrical fuel cell electrodes, were studied by synchrotron related techniques. The LSTC structure was characterized by X-ray powder diffraction showing a cubic Pm-3m and a

rhombohedric space group for the undoped (y = 0.0) and the Co-doped samples (0.0 < y ≤ 0.5), respectively. This loss of symmetry associated to the Co addition into the LST structure is due to the freezing of the $R5^-$ symmetry mode related to the rigid rotation of the oxygen octahedra around the transition metals. This result was confirmed by EXAFS, where no distortion was appreciable around the transition metals first coordination sphere. However, a noticeable difference was found comparing Ti and Co local environment along the LSTC series, since Ti-O distance remained stable at 1.91 Å while Co-O distance decreased with the Co content.

Perovskite A-site vacancies creation was found to be the active charge compensation mechanism for low Co-doped LSTC samples (y ≤ 0.3). Their concentration decreased with the increment of Co in the structure. No noticeable differences were found in the structural parameters with the grain size.

The combination between XANES experiments and DFT calculations allowed to evaluate the oxidation state of the transition metals in the LSTC samples. Ti formal valence remained close to 4+ for all compositions. Although the direct determination of the Co valence from the Co K-edge position was not possible, its comparison with reference materials established that the Co formal valence state must be close to 3+ in the studied samples.

Since the Ti is highly stable in a 4+ state, the introduction of Co in the structure with a 3+ formal valence state decreased the average B-site valence state providing extra electrons that were used for the incorporation of Sr inside the structure and, therefore, decreasing the A-site vacancies concentration.

LSTC characterization in working operation conditions as SSOFC electrode was performed with in-situ X-ray diffraction experiments. A reversible rhombohedric to cubic phase transition was found in all Co-doped LSTC samples. The transition temperature correlated with the room temperature rhombohedric distortion level. Ongoing XANES and EXAFS studies following the same conditions will show if there are any correlations between the structural transitions and electronic changes in the oxidation state.

Acknowledgments

This work has been supported by the Brazilian Synchrotron Light Laboratory (LNLS) unde proposals: XAFS1-11743, XAFS1 – 12800, XPD-11737 and XPD-12802, the Argentinean projects PICT-PAE 2288 and the PRH074 ANPCyT-CONICET and the BMBF-MinCyT binational cooperation agreement AL-10-10.

References

1. J. C. Ruiz-Morales, J. Canales-Vázquez, J. Peña Martínez, D. Marrero-López and P. Núñez, *Electrochimica Acta*, **52**(1), 278 (2006).
2. J. C. Ruiz-Morales, D. Marrero-López, J. Canales-Vázquez and J. T. S. Irvine, *RSC Advances*, **1**(8), 1403 (2011).

3. P. I. Cowin, C. T. G. Petit, R. Lan, J. T. S. Irvine and S. Tao, *Advanced Energy Materials*, **1**(3), 314 (2011).
4. J. Canales-Vázquez, J. C. Ruiz-Morales, D. Marrero-López, J. Peña Martínez, P. Núñez and P. Gómez-Romero, *Journal of Power Sources*, **171**(2), 552 (2007).
5. S. B. Adler, *Chemical Reviews*, **104**(10), 4791 (2004).
6. F. Napolitano, D. G. Lamas, A. Soldati and A. Serquis, *International Journal of Hydrogen Energy*, **37**, 18302 (2012).
7. F. Napolitano, A. L. Soldati, J. Geck, D. G. Lamas and A. Serquis, *International Journal of Hydrogen Energy*, **38**, 8965 (2013).
8. N. G. Eror and U. Balachandran, *Journal of Solid State Chemistry*, **40**(1), 85 (1981).
9. S. Hashimoto, L. Kindermann, F. W. Poulsen and M. A. Mogensen, *Journal of Alloys and Compounds*, **397**(1-2), 245 (2005)